Received: 15 May 2020 | Revised: 12 June 2020 | Accepted: 20 July 2020
DOI: 10.1002/qua.26426

FULL PAPER

International Journal of QUANTUM CHEMISTRY WILEY

Effects of rotational degree of freedom on calculations of photoassociation of HeH^+ systems

Bin-Bin Wang

Physics and Space Science College, China West Normal University, Nanchong, China

Correspondence
Bin-Bin Wang, Physics and Space Science College, China West Normal University, Nanchong 637009, China.
Email: binbinwang01@cwnu.edu.cn

Funding information
Fundamental Research Funds of China West Normal University, Grant/Award Number: 412775

Abstract

The role of rotational degree of freedom in calculations of photoassociation (PA) and the accompanying phenomena, that is, multiphoton transitions and above-threshold dissociations (PA-ATDs), of HeH^+ systems is investigated by comparing the numerical results of the one-dimensional (1D) and three-dimensional (3D) models in the framework of the time-dependent quantum wave packet method. It was found that the PA probability of the target state predicted by the 3D model is much smaller than that predicted by the 1D model. In addition, as the bound energies of interaction potential can be shifted by the inclusion of the rotational degree of freedom, the amplitude and frequency of optimized laser pulses obtained based on the 1D model should be changed to some extent to obtain maximal PA probability of the target state in realistic systems. The multiphoton transitions in the 3D case tend to be much easier to be excited. The variational behaviors of the PA-ATD probability vs the initial relative momentum of the two colliding particles, calculated in the 3D model using the optimized laser pulses obtained based on the 1D and 3D models, are found to be nearly coincident with each other, which implies that the continuum-continuum transitions from the initial wave packet tend to be the major dynamics in the PA-ATD process.

KEYWORDS

above-threshold dissociations, multiphoton transitions, photoassociation, rotational degree of freedom, time-dependent quantum wave packet method

1 | INTRODUCTION

With the experimental development of cold and ultracold atomic gases, the photoassociation (PA) process has received increasing attention in recent years.[1–3] This process provides a flexible means to prepare cold and ultracold molecules of particular interest directly from an assembly of laser-cooled atoms with the help of the external field.

In a general PA scheme, an intermediate bound level of the electronically excited state is first populated under the interaction of a pump laser field from a pair of initial colliding atoms in the ground electronic state. Then, the electronic ground-state molecule is obtained by either the spontaneous or stimulated emission. This scheme is particularly suited for creating an electronically ground bound state of homonuclear molecules, where no permanent dipole moment exists. For colliding atoms of dissimilar species, there exists another PA mechanism to obtain cold and ultracold electronically ground-state molecules, that is, prepare the molecule directly in the electronic ground state via the interaction with an infrared (IR) field.[4–12] This benefits from the nonnegligible permanent dipole moment of the heteronuclear systems.

As an important goal of this situation, high PA probability of the target state is always pursued. Korolkov et al. performed a calculation associated with PA of OH systems and found that the population of the target state can be controlled to reach its maximum by optimizing parameters

of the sin-squared laser pulse.[4] Since then, high PA probability of the heteronuclear systems, such as HI/HF,[5,13,14] HeH^+,[7,12] and CsLi systems,[11] has been theoretically obtained by either carefully designing the control schemes or optimizing the used laser pulses. In addition, due to the complex interaction of the laser pulse with the colliding atoms, some accompanying phenomena, such as multiphoton transitions and PA-relevant above-threshold dissociations (PA-ATDs), are also found in spite of relative weak laser fields adopted in the PA process.[9,12] These accompanying processes occur inevitably and tend to be important loss mechanisms under certain conditions, which prevents researchers from obtaining higher PA probability.

The PA and accompanying processes, mentioned above, are frequently investigated using the one-dimensional (1D) model,[4–9,11–15] that is, considering only the vibrational motion of the two colliding atoms, in the framework of the time-dependent quantum wave packet method. Based on the fact that the electric field coupling becomes the largest when the molecule axis is aligned parallel to the polarization direction of this field, this reduced-dimensional model is generally claimed to provide insight into the PA and dissociation processes in a full-dimensional case, that is, the three-dimensional (3D) model. However, the phenomena, predicted by the 1D model, and relevant numerical results, are always questioned by many theoretical researchers. This is because there are some deficiencies in the 1D model. For instance, as there is no consideration about the rotational degree of freedom, the rotational excitations could not be treated in this reduced-dimensional model. Therefore, whether such a simple 1D model could give a qualitative prediction about PA phenomena of the 3D case and how much the rotational degree of freedom will affect the numerical results of the 1D case tend to be interesting issues.

In this paper, based on the PA dynamics of HeH^+ systems and a prototype for the study of the PA dynamics,[7,12] the two mentioned issues are investigated by comparing the numerical results calculated using the 1D and 3D models. This can be also be viewed as an extension of our recent work,[12] where the PA phenomena is predicted in the 1D model for a wide range of collision energies by including the rotational degree of freedom. All the PA dynamics, including the PA process and the accompanying phenomena, that is, multiphoton transitions and dissociations, will be revisited in the 3D model. Atomic units are used throughout the paper, unless specified otherwise.

2 | METHODOLOGY

The PA reactions, steered by the IR laser pulse, are frequently investigated by solving either the 1D or the 3D time-dependent Schrödinger equation[4–17]

$$i\frac{\partial}{\partial t}\psi(t) = \hat{H}_x\psi(t), \quad x = \text{1D or 3D}, \tag{1}$$

with $\hat{H}_{1D}$ and $\hat{H}_{3D}$ denoting the Hamiltonians of the 1D and 3D models, respectively. Their explicit forms can be expressed as

$$\hat{H}_{1D} = \hat{T}_R + \hat{V} + \hat{W}_{int}^{1D} = -\frac{1}{2m}\frac{\partial^2}{\partial R^2} + V(R) - \mu(R)\varepsilon(t), \tag{2}$$

$$\begin{aligned}\hat{H}_{3D} &= \hat{T}_R + \hat{T}_\theta + \hat{V} + \hat{W}_{int}^{3D} \\ &= -\frac{1}{2m}\frac{\partial^2}{\partial R^2} - \frac{1}{2mR^2\sin\theta}\frac{\partial}{\partial\theta}\left(\sin\theta\frac{\partial}{\partial\theta}\right) + V(R) - \mu(R)\varepsilon(t)\cos\theta,\end{aligned} \tag{3}$$

where m is the reduced mass of the two colliding atoms, R the internuclear separation, and θ the angle between the molecular axis and the laser electric field. $V(R)$ and $\mu(R)$ are the ground potential energy and the permanent dipole moment of HeH^+ systems, respectively, which are taken from Tran.[18] $\varepsilon(t)$ denotes the laser pulse.

In both the model calculations, the $\sin^2$-shaped laser pulse is adopted, which is expressed as $\varepsilon(t) = f(t)\cos\omega(t - t_0) = \varepsilon_0\sin^2[\pi(t - t_0)/t_p]\cos\omega(t - t_0)$, with ε_0, ω, t_p, and t_0 denoting the laser-pulse peak amplitude, angular frequency, duration, and starting time, respectively. Note that, as this pulse is linearly polarized, the molecular magnetic quantum number M is conserved in the 3D model. Thus, the initial magnetic quantum number M is assumed to be zero, which is equivalent to ignoring the $\partial\varphi$ term (φ azimuthal angle). In addition, in Equation (1), the wave function $\psi(t)$ for the 1D model depends on two variables (R, t), while for the 3D model, it depends on three variables (R, θ, t).

The initial collision state in the 1D model is described by a typical Gaussian wave packet,[4–9,11–15] $\psi(R, t = 0) = (1/2\pi\delta^2)^{1/4}\exp[-ik_eR - (R - R_0)^2/4\delta^2]$, while in the 3D model, a product of this wave packet and the eigenfunction of the angular kinetic energy operator ($\hat{T}_\theta$), that is, the Legendre polynomial $\mathcal{P}_j(\theta)$, is necessary.[5,10,16] Just as in Marquetand and Engel,[5] Niu and Wang,[10] and Wang et al[16] the initial angular momentum quantum number j is set to be zero. We will also provide a simple discussion about the conditions where the initial wave packet is set to be higher j at the end of this work. In addition, to ensure that this initial wave packet is well located in the asymptotic domain, the initial central location R_0 and the width δ of this wave packet are set to 41 a.u. and 5 a.u., respectively. k_e denotes the initial (central) wave vector of the two

colliding atoms. In atomic units, the k_e has the same value as the corresponding collision momentum. Thus, for convenience, we will label k_e as the "collision momentum" in the following discussions.

With this initial wave packet in hand, Equation (1) can be easily solved using the split-operator method with the short time propagator,[19] that is,

$$\widehat{U}_{1D}(\Delta t) = e^{-i\widehat{H}_{1D}\Delta t} \approx e^{-i\widehat{T}_R\frac{\Delta t}{2}} e^{-i\left(\widehat{V}+\widehat{W}_{int}^{1D}\right)\Delta t} e^{-i\widehat{T}_R\frac{\Delta t}{2}}, \tag{4}$$

$$\widehat{U}_{3D}(\Delta t) = e^{-i\widehat{H}_{3D}\Delta t} \approx e^{-i\widehat{T}_R\frac{\Delta t}{2}} e^{-i\widehat{T}_\theta\frac{\Delta t}{2}} e^{-i\left(\widehat{V}+\widehat{W}_{int}^{3D}\right)\Delta t} e^{-i\widehat{T}_\theta\frac{\Delta t}{2}} e^{-i\widehat{T}_R\frac{\Delta t}{2}}, \tag{5}$$

where Δt is the short time step. The operators $\widehat{T}_R$ and $\widehat{T}_\theta$ are diagonal in the momentum space and the finite basis representation (FBR) of Legendre polynomials, respectively. Thus, in the calculation, $\widehat{T}_R$ is transformed between the momentum space and the coordinate space by using the fast Fourier transform method,[20] and $\widehat{T}_\theta$ is switched forward and backward between the FBR and the discrete variable representation (DVR) using Gauss-Legendre quadrature.[21] Of course, based on Equation (4), it is easy to note that the steps corresponding to $\widehat{T}_\theta$ described above do not need to be performed in the 1D model. The matrix $\widehat{V}+\widehat{W}_{int}^{3D}$ (or $\widehat{V}+\widehat{W}_{int}^{1D}$ in the 1D model) diagonalized in coordinate space (DVR) acts on the wave function directly in coordinate space by multiplication. It is also worth noticing that, in Equations (4) and (5), $\widehat{T}_R$ does not commute with $\widehat{V}+\widehat{W}_{int}^{1D}$ [$\widehat{T}_\theta$ or $\widehat{V}+\widehat{W}_{int}^{3D}$]; however, with the current treatment, the propagator is symmetrized, and the computational error has been checked and found to be very small with the short time step Δt.

In both calculations of the two models, the time step used for propagating the wave packet is 0.1 fs. The number of grids in R is set to 4096 for a box of $R \approx 300$ a.u. The Gauss-Legendre quadrature points used in θ are 40, which correspond to involving 40 rotational states in the 3D mode calculations, and the couplings among these rotational states steered by the laser pulse are well treated in the short time propagator, cf. Equations (4) and (5). In these settings, the results of both the PA and dissociation probability (see below) have been found to be converged at a minimum of five digits for all the initial collision conditions. In addition, the vibrational bound states are found to be 10 for HeH^+ systems.

In the 3D model, the rovibrational state $|v, j\rangle$ is a direct product of $\mathcal{P}_j(\theta)$ and the j-dependent (radial) vibrational function $\phi_{v,j}(R)$, while in the 1D model, only the vibrational state $|v\rangle$, that is, the vibrational function $\phi_v(R)$, is needed. Both $\phi_v(R)$ and $\phi_{v,j}(R)$ are calculated numerically by solving the time-independent Schrödinger equation using the Fourier grid Hamiltonian method[22]:

$$\left[-\frac{1}{2m}\frac{\partial^2}{\partial R^2} + V(R)\right]\phi_v(R) = \varepsilon_v\phi_v(R), \tag{6}$$

$$\left[-\frac{1}{2m}\frac{\partial^2}{\partial R^2} + \frac{j(j+1)}{2mR^2} + V(R)\right]\phi_{v,j}(R) = \varepsilon_{v,j}\phi_{v,j}(R). \tag{7}$$

In the above equations, ε_v and $\varepsilon_{v,j}$ denote the vibrational and rovibrational energies in the 1D and 3D models, respectively. Note that the difference between ε_v and $\varepsilon_{v,j}$ is an important factor in determining the deviation of numerical results about the PA process based on the 3D model from those based on the 1D model.

Then, the PA probability of a selected bound state is obtained by projecting the wave function $\psi(t)$ on it, and the total PA probability is simply the sum of the PA probability of each bound state. For the 1D model, these read as follows:

$$P_v(t) = |\langle v|\psi(t)\rangle|^2, \text{ and } P_{total}(t) = \sum_v P_v(t), \tag{8}$$

while for the 3D model, they are written as

$$\widetilde{P}_{v,j}(t) = |\langle v,j|\psi(t)\rangle|^2, \text{ and } \widetilde{P}_{total}(t) = \sum_v\sum_j \widetilde{P}_{v,j}(t). \tag{9}$$

Comparing the numerical results of the two models, the PA probability associated with a selected vibrational state is also calculated in the 3D model, which reads $\widetilde{P}_v(t) = \sum_j \widetilde{P}_{v,j}(t)$. Note that all the numerical results based on the 3D model are highlighted by the wavy line symbol, that is, "$\sim$".

Alongside the PA process, dissociation also takes place, and its probability can be calculated by the projection method,[23,24] that is,

$$D(E_i) = |\langle E_i|\psi(t_{\text{final}})\rangle|^2,\ \tilde{D}(E_{i,j}) = |\langle E_{i,j}|\psi(t_{\text{final}})\rangle|^2, \tag{10}$$

where $|E_i\rangle$ and $|E_{i,j}\rangle$ denote the box-normalized quasicontinuum states in the 1D and 3D models, respectively. Here, $t = t_{\text{final}}$ denotes that the dissociation is calculated at the end of the interaction laser pulse. Then, the total PA-ATD probability is obtained by summing relevant parts, that is,

$$D_{\text{PA-ATD}} = \sum_{i \geq n_0} D(E_i),\ \text{and}\ \tilde{D}_{\text{PA-ATD}} = \sum_{i \geq n_0}\sum_{j} \tilde{D}(E_{i,j}), \tag{11}$$

where n_0 denotes the dissociation boundary, above which the energy of the corresponding (dissociation) fragments is at least one photon larger than the initial collision energy.

3 | RESULTS AND DISCUSSIONS

To investigate the difference of the 1D and 3D models in calculating the PA probability associated with the target state $v = 6$, the optical laser pulses obtained based on the 1D model in our previous work[12] are directly used to drive the PA process in the 3D model. To obtain such an optical laser pulse in the 1D model (and also in the 3D model, see the following discussions), all the laser parameters, namely, the laser pulse peak amplitude, central frequency, duration, and starting time, should be optimized, which includes several steps.[13,25]

As an initial choice, we set the pulse central time to be the moment when the (time-dependent) coupling between the collision wave packet and the target state reaches its maximum, and the pulse duration to be comparable with the time interval when the coupling presents a relatively large value. The central frequency is determined by the energy difference between the initial wave packet and the target state. The peak intensity of the laser pulse is first altered to obtain a maximal final PA probability of the target state. Then, the central frequency of the pump pulse is scanned to find an optimal value due to one-photon detuning. Thereafter, the pulse duration and the central time are optimized to obtain the maximal PA probability of the target state. Through the steps stated above, one iteration of the optimal process is finished. Such an iteration is repeated till the PA probability of the target state converges, that is, the final PA probability of the target state reaches its maximal value and remains unchanged. Note that the starting time of the laser pulse can be easily obtained from the pulse central time and duration, and the results relevant to the PA probability, given by our optimizations, are converged to at least two significant digits, as are the results of accompanying multiphoton transitions and dissociations.

The numerical result is shown in Figure 1A, along with the PA probability based on the 1D model. As shown, although the same laser pulse is adopted for the two models at each initial collision momentum k_e, there exist many differences between the numerical results. First, as the laser pulse is optimized in the 1D model, the PA probability of both the target and total bound states based on the 3D model is much smaller than that based on the 1D model for each k_e. Second, the variation behavior of the PA probability vs k_e predicted by the 1D model almost no longer persists in the 3D model. Actually, the two models only give a similar prediction about the increasing behavior of the PA probability for $k_e \geq 3.5$ a.u. Finally, the initial collision condition and intensity associated with the multiphoton transitions predicted by the 1D model are also relatively

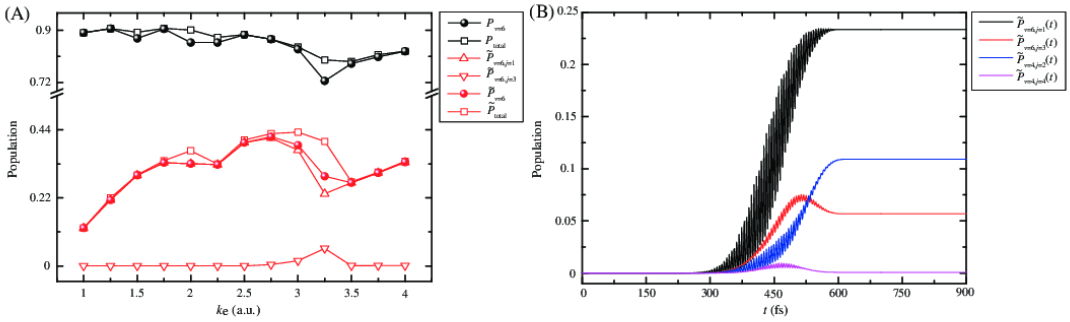

FIGURE 1 A, Comparison of numerical results for the final PA probability of the target states, that is, the bound states associated with $v = 6$, based on the 1D and 3D models. The laser pulse used is the same for a given k_e in the two models, while it is only optimized in the 1D model, cf. Jing et al[12] for parameters of such laser pulse. B, The time-dependent population at $k_e = 3.25$ a.u. in the 3D model

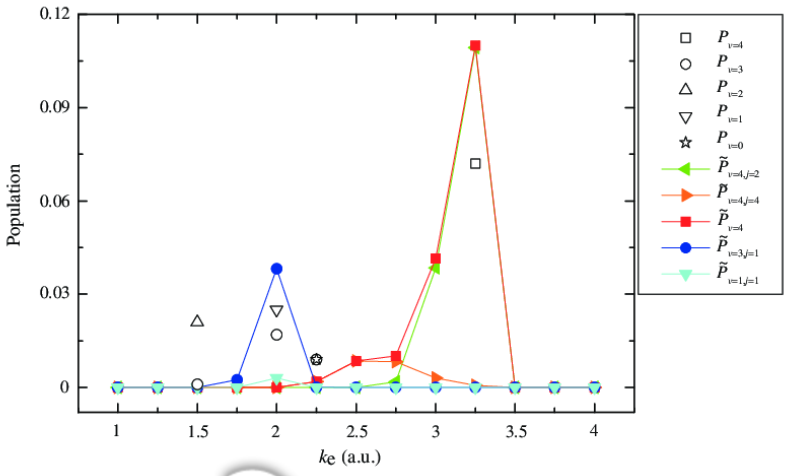

FIGURE 2 Comparison of numerical results associated with the accompanying main multiphoton transitions in the 1D and 3D models. The laser pulse used is the same for a given k_e in the two models, while it is only optimized in the 1D model

different from those predicted by the 3D model. Note that the multiphoton transitions described above can be roughly identified from the non-negligible difference between the total bound state and the target state; cf. also Figure 2 for such multiphoton transitions.

In addition, it is also worth noticing that, in the 3D model, two main rotational states associated with the target state $v = 6$ are involved at $k_e = 3.25$ a.u., that is, the states with the rotational quantum numbers $j = 1$ and 3. The transition from the initial wave packet, in which the rotational number is set to be zero, to the former rovibrational state $(v, j) = (6, 1)$ corresponds to the one-photon transition process, and meets the transition selection rule, $\Delta j = \pm 1$. However, the population of the latter rovibrational state (6, 3) is related to either a Raman transition ($\Delta j = 2$) from the former state (6, 1) or a three-photon transition directly from the initial wave packet. Note that the Raman transition can be also viewed as a two-photon transition process. These transitions tend to be strongest at $k_e = 3.25$ a.u., where multiphoton transitions associated with other bound states are also the largest. Figure 1B shows the time-dependent PA process based on the 3D model at such initial collision momentum, that is, $k_e = 3.25$ a.u. As can be seen, the one-photon PA process from the initial collision wave packet to the rovibrational state (6, 1) first takes place near 250 fs. Then, about 50 fs later, the rovibrational states (6, 3) and (4, 2) are almost simultaneously populated via the multiphoton transitions. The rovibrational state (4, 4) is also excited to some extent near 450 fs. At the end of the laser pulse, the PA probability associated with the multiphoton transitions, that is, the PA probability of (6, 3) and (4, 2), contributes greatly to the total PA probability.

The main multiphoton transitions associated with other bound states are shown in Figure 2. As can be seen, only the strongest multiphoton transitions at $k_e = 2$ and 3.25 a.u., predicted by the 1D model, correspond to the nonnegligible multiphoton ones in the 3D model. However, both the vibrational states $v = 3$ and 1 are considerably populated, and the PA probability of $v = 1$ is a little larger at $k_e = 2$ a.u. in the 1D model. This is different from the case predicted by the 3D model, where the rovibrational state (3, 1) tends to be mainly populated, and the PA probability of (1, 1) is much smaller. At $k_e = 3.25$ a.u., the multiphoton transition predicted by the 3D model is much stronger than the one predicted by the 1D model.

All the disagreements described above may be ascribed partly to the energy shift of the target state by the rotational degree of freedom. This energy shift is equal to the energy difference between (6, 0) and (6, 1), which is about 33 cm^{-1}. To investigate its role in determining the discrepancy of PA phenomena predicted by the 1D and 3D models, the laser pulse used in the 3D model is also optimized for each k_e. The optimization procedure is the same as the one performed based on the 1D model.[7,12] The peak amplitudes and detunings of our obtained laser pulses for different k_e are shown in Figure 3A,B, respectively. In these figures, those corresponding to the 1D model are also given for comparison. Furthermore, it should be noted that the detuning for the two models in this work is first defined referring to the energy difference between the initial wave packet and the target state $v = 6$ in the 1D model, that is, $\Delta = \hbar\omega - (E - \varepsilon_{v=6})$, with $\hbar\omega$ and E denoting the photon energy of the adopted laser pulse and the collision energy of the initial wave packet, respectively.

As can be seen, although the two groups of laser pulses are optimized based on different models, the variation behaviors of peak amplitudes and detunings of these pulses vs k_e closely follow each other. There, of course, exist some differences. The peak amplitude of the laser pulse optimized based on the 3D model is a little larger than the one based on the 1D model, which implies that a stronger laser pulse should be adopted to steer the complex PA process in a realistic system. In addition, the energy shift caused by the rotational degree of freedom, that is, 33 cm^{-1}, should be subtracted in the detuning of the 3D model to make its variation behavior vs k_e much similar with the one based on the 1D model. In other words, if the detunings of the laser pulses in the 3D and 1D models are defined as $\Delta = \hbar\omega - (E - \varepsilon_{v=6,\ j=1})$ and $\Delta = \hbar\omega - (E - \varepsilon_{v=6})$, respectively, the variation behaviors of the detunings vs k_e in the two models will follow each other more closely, cf. the red open circles and black solid

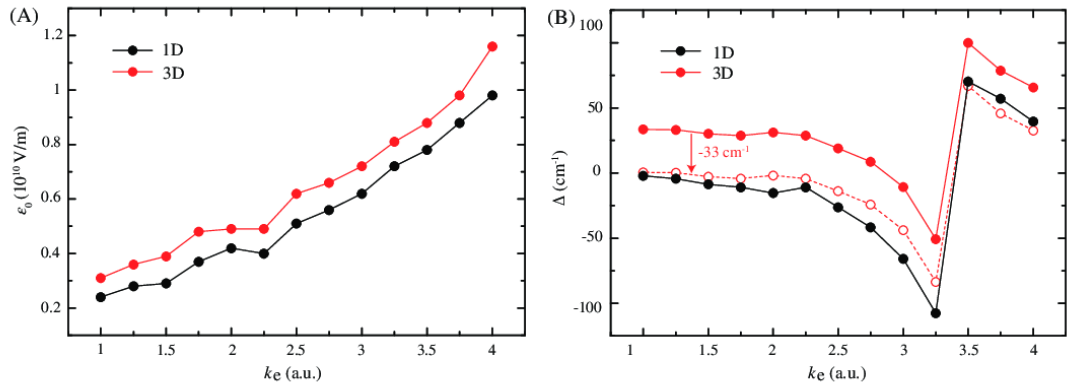

FIGURE 3 Comparison of peak amplitudes, A and detunings, B, of the laser pulses that were optimized, respectively, in the 1D and 3D models. The red open circles in the right panel correspond to the detunings of the optical laser pulses associated with the 3D model minus 33 cm^{-1}. These detunings are first defined referring to the energy difference between the initial wave packet and the target state $v = 6$ in the 1D model—see the main text. The energy of the target state $v = 6$ in the 1D model is −2191.701 cm^{-1}

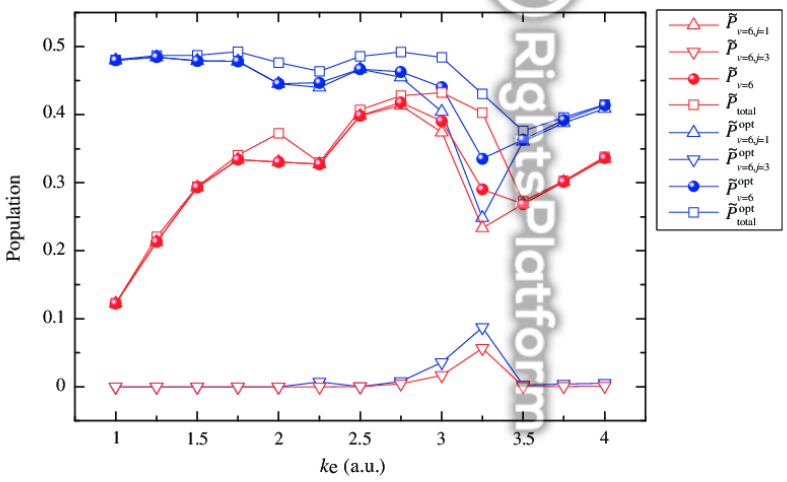

FIGURE 4 Comparison of numerical results about the final population of the target and total bound states in the 3D model but based on two groups of laser pulses that correspond to the ones optimized in the 1D (red symbols) and 3D (blue symbols) models, respectively

balls in Figure 3B. For the durations and starting times of the optical laser pulses in the 3D model (not shown), they are found to be consistent with those predicted by the 1D model, which may be ascribed to roughly the same coupling between the collision wave packet and the target state in the field free condition in the two models.[12] In practice, as found in Jing et al,[12] the full width at half maximums (FWHMs) of the optimal laser pulse is 1.35 times as long as the FWHMs, τ_{FC}, of the coupling between the collision wave packet and the target state in the field free condition. The central time of the optimized laser pulse is found to occur near $0.35\tau_{FC}$ before the coupling between the collision wave packet and the target state reaches its maximum. Note that the FWHM of the $\sin^2$-shaped laser pulse is half its duration.

Figure 4 shows numerical results based on the two groups of optical laser pulses that are applied in the 3D model. Note that all the PA phenomena associated with the laser pulse optimized based on the 3D model will be labeled by the superscript "opt". As can be seen, when the laser pulse optimized based on the 3D model is considered, the PA probability of both the target and total bound states increases greatly for most k_e, particularly for $k_e < 2.5$ a.u. This is because of the relatively smaller detunings of the optical laser pulses for these initial collision energies, cf. Figure 3B. Therefore, when the optical laser pulse that was optimized based on the 3D model is applied, both the PA probability and its variation behavior vs k_e predicted by the 1D model tend to revive to some extent, cf. Figures 1A and 4. Of course, the 1D model still overestimates the PA probability of the target and total bound states by about one time. In addition, the multiphoton transitions tends to be much easier to occur for most k_e in the 3D case.

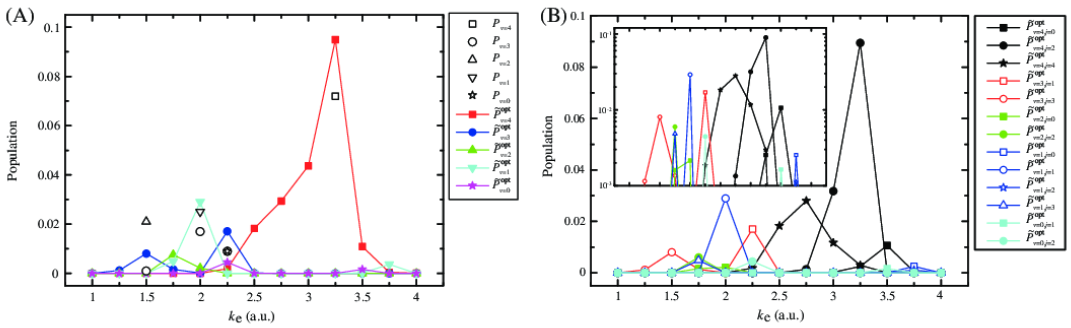

FIGURE 5 A, Comparison of numerical results based on the 1D and 3D models about the probability of main multiphoton transitions. B, The detailed information about the rotational excitations corresponding to the main multiphoton transitions in the 3D model. The laser pulses used in either the 1D or 3D models are the corresponding optical ones

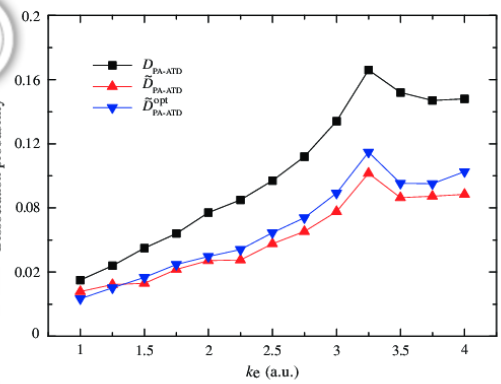

FIGURE 6 Comparison of numerical results about the accompanying PA-ATD probability. Two groups of laser pulses are used: one group of these is the optical laser pulses obtained in the 1D model, applied to the 1D (black squares) and 3D models (red up triangles). The other are the ones optimized and used in the 3D model (blue down triangles). ATD, above-threshold dissociation; PA, photoassociation

The main multiphoton transitions to other bound states are shown in Figure 5. In Figure 5A, the optical PA probability predicted by the 1D model is also displayed for comparison. As can be seen, although there are still many differences between the main multiphoton transitions predicted by the two models, the multiphoton transitions predicted by the 1D model tend to revive to some extent, cf. Figures 2 and 5A. For instance, all the main multiphoton transitions predicted by the 1D model tend to also be cases of multiphoton transitions in the 3D model. Figure 5B shows detailed information about these multiphoton transitions in the 3D model. As shown, more than two rovibrational states are excited for most cases of these multiphoton transitions, which may be ascribed to the larger bandwidth of the applied laser pulse than the spacing of the relevant rovibrational states, cf. our previous work.[12]

Now, we discuss the difference of the numerical results between the two models in calculating the PA-ATD probability. Here, three cases of numerical results about the PA-ATD probability are considered and compared. Two are based on the 3D model but using different groups of optical laser pulses, that is, the one optimized in the 1D model and the one optimized in the 3D model. The third case is the numerical result calculated based on the 1D model and using the corresponding optical laser pulse. As shown in Figure 6, although the PA probability, which is based on two different optical laser pulses in the 3D model, differs greatly (cf. Figure 4), the amplitude and variation behavior of the PA-ATD probability vs k_e are almost the same. This implies that the transitions via the molecular bound states have little impact on the PA-ATD process for most k_e, and continuum-continuum transitions from the initial wave packet do contribute greatly to the PA-ATD process.

Of course, the small correlation of the transitions via molecular bound states to the PA-ATD process can be also identified from the relative variations of PA-ATD probability that are based on the two different optical lasers for $k_e < 2.5$ a.u. In addition, from the comparison of the PA-ATD probability based on the two groups of optical laser pulses in the 3D model and those based on the 1D model, it could be found that the 1D model does give a relatively correct prediction about the PA-ATD probability and its variation behavior vs k_e. In particular, the enhancement of the PA-ATD process at $k_e = 3.25$ a.u. using the strong multiphoton transitions is obviously shown in all the three cases, which implies that the 1D model is successful in predicting such a novel process.

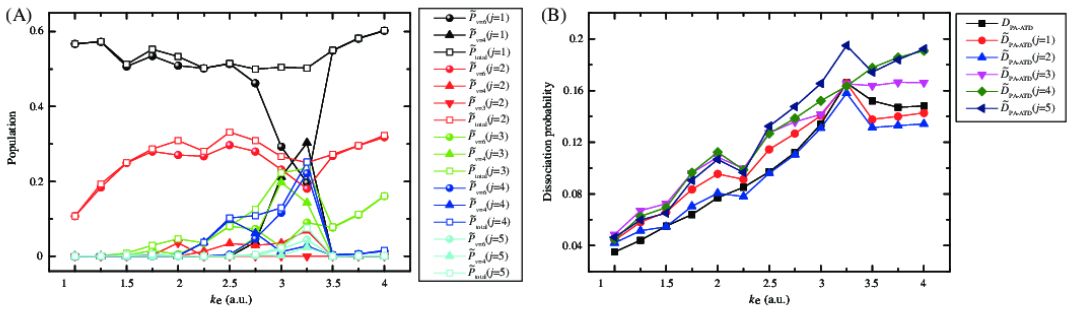

FIGURE 7 The numerical results based on the 3D model about the PA, A and PA-ATD, B, probability for initial wave packets with higher rotational quantum number *j*. In the right panel, the numerical results about the PA-ATD probability based on the 1D model are also shown and are denoted by the black squares. The laser pulses used are the optical ones obtained in the 1D model. ATD, above-threshold dissociation; PA, photoassociation

Finally, to complete this investigation, the optical laser pulse obtained based on the 1D model is also applied directly in the 3D model for the initial wave packet with higher rotational wave numbers, that is, with *j* running from 1 to 5. The numerical results are shown in Figure 7. Figure 7A displays the variation behaviors of the PA probability vs k_e for these cases. As can be seen, with the increase of *j*, the PA probability of both target and bound states changes greatly for each k_e. This implies that the PA probability of HeH^+ systems will be affected greatly by thermal averaging. The variation behaviors of the PA-ATD probability for these cases vs k_e are given in Figure 7B. For comparison, the PA-ATD probability predicted based on the 1D model is also given in this figure. As shown, although the numerical results based on the 3D model differ from those based on the 1D model, the variation behavior of PA-ATD probability vs k_e predicted by the 1D model does persist in the realistic systems, that is, in the 3D case. In addition, in contrast to the case of the PA probability, the PA-ATD probability and its variation behavior in the 3D model for different *j* closely follow each other. This implies that an explicit thermal averaging will not significantly change the PA-ATD probability and its variation behavior.

4 | CONCLUSION

In this paper, the effects of rotational degree of freedom on calculations of the PA and accompanying phenomena of HeH^+ systems are investigated by comparing the numerical results of 1D and 3D models. It is found that the PA probability of the target state predicted by the 1D model is much larger than that predicted by the 3D model. In addition, as the bound energies of interaction potential can be shifted by the inclusion of the rotational degree of freedom, the amplitude and frequency of optimized laser pulses obtained based on the 1D model should be changed to some extent to obtain maximal PA probability of the target state in realistic systems.

For the cases of multiphoton transitions, the 1D model could only give a qualitative prediction about some multiphoton transitions, and the multiphoton transitions in the 3D case tend to be much easier to excite. For the PA-ATD phenomena, the 1D model does give a quantitative prediction. Furthermore, the continuum-continuum transitions from the initial wave packet tend to be the major dynamics in the PA-ATD process, and thermal averaging has little effect on the numerical results of the PA-ATD probability in the 3D model.

In the end, although the state $v = 6$ is chosen as the target state, the findings in this work are expected to be applicable to other target states of this system and other systems, particularly the findings relevant to the PA-ATD phenomena. This can be understood from the fact that the continuum-continuum transitions from the collision wave packet contribute greatly to the PA-ATD dynamics, and the continuum-energy spectra tend to be the same for a given system and similar for different systems. For the PA process, the validity of our findings to other target states or other systems can be accounted for by the similar structure of the rotational levels associated with each vibrational state. Of course, the numerical results of the PA process are also expected to be related to the detailed information of these rotational states, for example, the spacing of the adjacent rovibrational levels near the target state. Therefore, these findings, relevant to the PA process in this work, are more suited for the interaction potentials similar to those of HeH^+ systems. Actually, the numerical results of the PA phenomena predicted by the 1D and 3D models associated with the target state $v = 6$ of the HeD^+ system are also compared (not shown), and they present the same findings. The system dependence of our findings in this work is an intriguing issue, and we expect that it will receive more investigations in the future.

ACKNOWLEDGMENTS

The project was supported by the Fundamental Research Funds of China West Normal University (No. 412775).

AUTHOR CONTRIBUTIONS

Bin-Bin Wang: Investigation; writing-original draft.

ORCID

Bin-Bin Wang https://orcid.org/0000-0003-3683-6910

REFERENCES

[1] K. M. Jones, E. Tiesinga, P. D. Lett, P. S. Julienne, *Rev. Mod. Phys.* **2006**, *78*, 483.
[2] C. P. Koch, M. Shapiro, *Chem. Rev.* **2012**, *112*, 4928.
[3] J. Ulmanis, J. Deiglmayr, M. Repp, R. Wester, M. Weidemüller, *Chem. Rev.* **2012**, *112*, 4890.
[4] M. V. Korolkov, B. Schmidt, *Chem. Phys. Lett.* **1997**, *272*, 96.
[5] P. Marquetand, V. Engel, *J. Chem. Phys.* **2007**, *127*, 084115.
[6] E. F. de Lima, T.-S. Ho, H. Rabitz, *Phys. Rev. A* **2008**, *78*, 063417.
[7] Y.-Y. Niu, R. Wang, M.-H. Qiu, J.-L. Xiu, *Int. J. Quantum Chem.* **2011**, *111*, 2117.
[8] E. F. de Lima, T.-S. Ho, H. Rabitz, *Chem. Phys. Lett.* **2011**, *501*, 267.
[9] Y.-C. Han, *Laser Phys. Lett.* **2017**, *14*, 125302.
[10] Y.-Y. Niu, R. Wang, *Chin. Opt. Lett.* **2018**, *16*, 060201.
[11] I. C. de Almeida, E. F. de Lima, *Laser Phys.* **2019**, *29*, 035501.
[12] S.-H. Jing, B.-B. Wang, X.-Y. Zhou, T.-X. Zeng, *Int. J. Quantum Chem.* **2020**, *120*, e26196.
[13] Y.-Y. Niu, S.-M. Wang, S.-L. Cong, *Chem. Phys. Lett.* **2006**, *428*, 7.
[14] P. Shen, Y.-C. Han, J.-L. Li, K. Yi, C. Chen, S.-L. Cong, *Laser Phys. Lett.* 2015, *12*, 045302.
[15] E. F. de Lima, *Phys. Rev. A* **2017**, *95*, 013411.
[16] B.-B. Wang, Y.-C. Han, S.-L. Cong, *J. Chem. Phys.* **2015**, *143*, 094303.
[17] Y.-C. Han, *Int. J. Quantum Chem.* **2019**, *119*, e25858.
[18] P. Tran, *Phys. Rev. A* **1999**, *59*, 1444.
[19] M. D. Feit, J. A. Fleck Jr., A. Steiger, *J. Comput. Phys.* **1982**, *47*, 412.
[20] D. Kosloff, R. Kosloff, *J. Comput. Phys.* **1983**, *52*, 35.
[21] J. C. Light, I. P. Hamilton, J. V. Lill, *J. Chem. Phys.* **1985**, *82*, 1400.
[22] C. C. Marston, G. G. Balint-Kurti, *J. Chem. Phys.* **1989**, *91*, 3571.
[23] P. Lambropoulos, P. Zoller, *Phys. Rev. A* **1981**, *24*, 379.
[24] X. Tang, H. Rudolph, P. Lambropoulos, *Phys. Rev. Lett.* **1990**, *65*, 3269.
[25] B.-B. Wang, Y.-C. Han, Y.-H. Pang, S.-L. Cong, Y.-Y. Niu, *Theor. Chem. Acc.* **2015**, *134*, 80.

How to cite this article: Wang B-B. Effects of rotational degree of freedom on calculations of photoassociation of HeH^+ systems. *Int J Quantum Chem*. 2021;121:e26426. https://doi.org/10.1002/qua.26426